



Darcy-Reynolds forces during intrusion into granular-fluid beds

Joshua Strader ¹, Neil Causley,¹ Joshua A. Dijksman,² and Abram H. Clark ¹

¹*Department of Physics, Naval Postgraduate School, 833 Dyer Road, Monterey, California 93943, USA*

²*Physical Chemistry and Soft Matter, Wageningen University and Research, Stippeneng 4, 6708 WE Wageningen, the Netherlands*



(Received 25 July 2021; accepted 17 May 2022; published 31 May 2022)

We experimentally study intrusion into fluid-saturated granular beds by a free-falling sphere, varying particle size and fluid viscosity. We test our results against Darcy-Reynolds theory, where the deceleration of the sphere is controlled by Reynolds dilatancy and the Darcy flow resistance. We find the observed intruder dynamics are consistent with Darcy-Reynolds theory for varied particle size. We also find that our experimental results for varied viscosity are consistent with Darcy-Reynolds theory, but only for a limited range of the viscosity. For large viscosities, observed forces begin to decrease with increasing viscosity, in contrast with the theoretical prediction. We suggest that a dynamic lubrication mechanism may be responsible for the observed discrepancy.

DOI: [10.1103/PhysRevFluids.7.054304](https://doi.org/10.1103/PhysRevFluids.7.054304)

I. INTRODUCTION

Intrusion or impact into a granular-fluid mixtures is a common process with relevance in, e.g., bio-inspired locomotion problems [1,2] or shock absorption applications [3]. Each of the constituent phases of this system (granular flows or fluid flows) is already challenging enough to describe, and the combination is even more difficult. There has been extensive recent work on steady-state rheology of granular fluid mixtures, including generalizations of inertial rheology descriptions for granular flows [4–7] as well as rheological studies of shear-thickening behavior [8–10]. Steady-state analyses of granular and suspension flows often assume a weak coupling between the dynamics of both phases or only mild gradients (space or time) in the flow rate or the local stress. These analyses therefore offer few handles to understand more complex flow situations such as intrusion, which inherently involves compaction or dilation and propagation phenomena [11–14]. Thus, in addition to the utility of describing the impact or intrusion process for practical applications, intrusion is a useful benchmark to probe the limits of existing theories and uncover new physics. This has been recognized by a diverse and expanding set of works on intrusion [12,15–17]. In particular, understanding how relevant data during an impact (e.g., crater size [18,19] or peak forces [15,20]) depends on system parameters (e.g., intruder speed, intruder size, or grain stiffness) often yields significant insight about underlying physics, especially inherently transient processes that by definition cannot be captured by steady-state descriptions.

A notable example of such a process was recently highlighted by Jerome *et al.* [21]. When intrusion occurs into a granular bed in which the packing fraction ϕ is compacted above a critical volume fraction ϕ_c (due to, e.g., external vibrations [22,23] or aging from other mechanisms [24,25]), there is an initial transient where the bed dilates, due to Reynolds dilatancy [26]. Generally, the bed will be saturated in some fluid (e.g., air or water), and the fluid will be sucked into the expanding pore structure. For sufficiently small particles and a sufficiently viscous fluid, Darcy pressure [27] begins to play an increasingly dominant role during the granular bed expansion. Jerome *et al.* [21] formulated a basic theory that combined these two effects, called Darcy-Reynolds theory (DRT), to

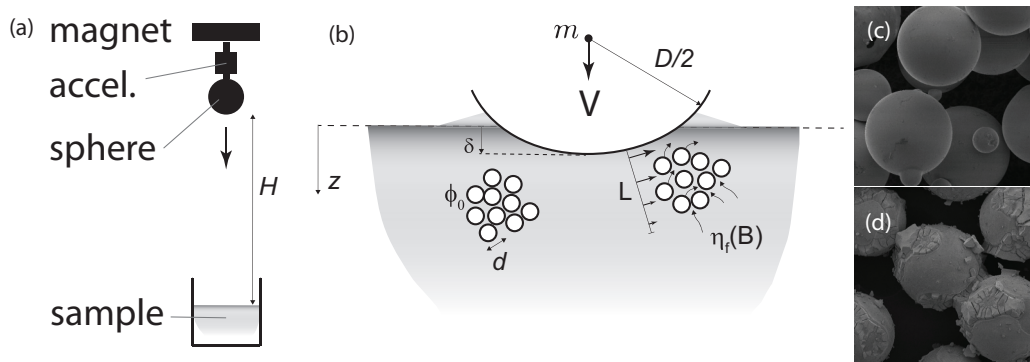


FIG. 1. (a) Sketch of the experiment. The magnet releases the sphere, which is connected to the accelerometer (accel.) via a threaded rod. The magnet is released at height H onto the submerged settled particle bed (sample). (b) Sketch of the particle bed slowing down the spherical intruder impacting the bed of particles with diameter d and packing fraction ϕ_0 . The penetration of the intruder with speed V , diameter D , and mass m will make the particles bulge out from the bed surface (long dashed line). At penetration depth $z = \delta$ the particles have been sheared in a region with size L . This shear required dilation of the packing and thus forces the local absorption of fluid with viscosity $\eta_f(B)$ whose properties may depend on the applied magnetic field strength B . (c) SEM image of the glass beads used, showing slight polydispersity and a mild roughness (d) SEM image of dried ferrofluid on the glass beads. The individual ferrofluid nanoparticles are too small to observe, yet the leftovers from capillary bridges are clearly visible. Image width in (c) and (d) is $200 \mu\text{m}$.

describe the dynamics of spheres impacting granular beds that were fully immersed in a fluid. The authors showed explicitly that DRT could explain the dependence on ϕ of the force response during intrusion into fluid-saturated granular beds.

Although the ϕ dependence of the impact response was confirmed to agree with DRT [21], several other parameters like viscosity η_f of the interstitial fluid or the particle diameter d play a crucial role in this theory, but the scaling behavior for these parameters was tested only for a few cases. If tested and confirmed, this would provide a framework that could be used for, e.g., prediction of robotic locomotion behavior [28,29] or tunable granular-fluid mixtures. One particular example motivating this study is the use of a ferrofluid as the viscous fluid. Ferrofluids [30] consist of nanometer-sized iron particles coated in a surfactant suspended in a simple fluid (e.g., alcohol or a petroleum-based fluid). Ferrofluids behave approximately as Newtonian viscous fluids, but with a viscosity that depends on the applied magnetic field. Thus, the viscosity can be changed *in situ* during the use of the material to achieve a desired mechanical response. Since Darcy-Reynolds pressure increases with increasing η_f , this could provide a way to externally tune the flow behavior of granular-fluid mixtures.

Here we demonstrate how DRT predicts scaling laws for intrusion into fluid-grain mixtures as a function of particle size and fluid viscosity. We then experimentally test these scaling laws with impact experiments by dropping spheres from a height H into fluid-saturated granular beds with varying particle size d and fluid viscosity η_f ; see Fig. 1(a). In both cases we find results that are consistent with DRT over a range of parameter values. We observe some change to the phenomenology for large d ; we show that this can be explained using DRT. However, we also observe a qualitative discrepancy for the predicted behavior for large η_f which cannot be reconciled with DRT. Increasing η_f should lead to increasing Darcy-Reynolds forces. Instead, we observe that for large η_f , increasing η_f leads to decreasing forces during impact. Viscosity is controlled by adding glycerol to water as well as by using a ferrofluid and tuning the viscosity with an external applied magnetic field; both methods yield similar results. Our results demonstrate that DRT as formulated describes variation in d over a wide range but breaks down for large viscosities, at least

for the particles and fluids studied here. However, the overall agreement between the glycerol-water mixtures and the ferrofluid suggest that ferrofluids could be used to construct tunable complex fluids, where the applied magnetic field controls the viscosity and hence impacts hardness.

II. DARCY-REYNOLDS THEORY

We first reproduce the derivation of DRT that appears in the main text and the Supplemental Material of Jerome *et al.* [21]. The key idea is that intrusion of an object requires shear in the particulate phase. Such shear gives rise to frictional stress as set by some effective friction coefficient. Additionally, when a packing is denser than its “critical state” solid fraction ϕ_c —i.e., the density it would have during steady-state shear—then the material will dilate when sheared until asymptotically approaching ϕ_c , a process known as Reynolds dilatancy. This induces fluid flow into the expanding pores. Under certain conditions the pore fluid pressure P_f can locally reach values much larger than any other local pressure scale, such as gravity, in which case P_f dominates the dynamics. The key hurdle is then to find an expression for P_f for the situation sketched in Fig. 1(b).

It is reasonable to assume that the rate of dilation is linearly proportional to the shear rate $\dot{\gamma}$ [31]. Thus, the first assumption of this theory is that the dilation obeys a simple differential equation,

$$\frac{1}{\phi} \frac{\partial \phi}{\partial t} = -\alpha \dot{\gamma} (\phi - \phi_c). \quad (1)$$

To approximate the magnitude of α , we take finite differences, i.e., $\dot{\gamma} \rightarrow \delta\gamma/\delta t$. We assume that the strain needed over which dilation happens is $\delta\gamma \approx 0.1$ [31–33], and $\partial\phi/\partial t \rightarrow \delta\phi/\delta t$, with $\delta\phi \approx \phi_c - \phi$, yielding $\alpha = 1/(\phi\delta\gamma)$. If $\phi \approx 0.6$, then $\alpha \approx 20$. We use this approximation later to confirm that our comparison between theory and experiments is reasonable.

As previously stated, when the granular phase dilates, fluid from elsewhere in the material must fill this volume opened up via dilation. If the particle diameter d is small and/or the fluid viscosity η_f is large, then the Darcy flow resistance of the fluid through the pore structure is dominant. The Darcy law states that

$$(1 - \phi)(\mathbf{V}_f - \mathbf{V}_p) = -\frac{\kappa}{\eta_f} \nabla P_f, \quad (2)$$

where $\kappa \propto d^2$ is the permeability, η_f is the fluid viscosity, and P_f is the pore pressure. Assuming that the particle and fluid phases are both incompressible, i.e., $\partial\phi/\partial t + \nabla \cdot (\phi\mathbf{V}_f) = 0$ and $\partial\phi/\partial t + \nabla \cdot (\phi\mathbf{V}_p) = 0$, then taking the divergence of Eq. (2) yields $(1/\phi)\partial\phi/\partial t = -(\kappa^2/\eta_f)\nabla^2 P_f$, assuming that spatial dependence in ϕ can be neglected (i.e., $\nabla\phi = 0$). Combining with Eq. (1) yields

$$\nabla^2 P_f = \frac{\eta_f}{\kappa} \alpha \dot{\gamma} (\phi - \phi_c). \quad (3)$$

This equation represents a local constitutive law, which can then be extended to impact of a sphere into a saturated granular bed, with initial volume fraction ϕ_0 , using several more assumptions. During impact, there is a shearlike deformation that occurs beneath the intruder. The first important assumption is that this shear deformation occurs over a length scale L , which is proportional to the square root of the *instantaneous* contact area between the intruder and the fluid-grain mixture. In this picture, P_f then sets the pressure scale for a frictional intrusion-resisting force. The fact that the instantaneous contact area determines the shear length scale represents a qualitative difference between DRT and recent theories that have been proposed to describe impact into dense suspensions, where propagating dynamically jammed fronts play a crucial role [12,14,16,34]. Something like DRT likely describes why these these dynamically jammed fronts remain solidified, due to very small (e.g., cornstarch) particles with very low associated permeability. These two systems (fluid-saturated granular beds and dense suspensions) have obvious similarities, but this and other key differences make direct comparisons challenging; we discuss this further at the end of Sec. VI.

A. The role of shear length scale L

Assuming that the shear length scale L is set by the square root of the contact area between the ball and the material, the shear rate is $\dot{\gamma} \sim v/L$, where v is the speed of the intruder. The pore-pressure effects also act over length scale L , so $\nabla^2 P_f \sim P_f/L^2$. Thus, Eq. (3) becomes

$$P_f \sim \frac{\eta_f}{d^2} \alpha L v (\phi - \phi_c), \quad (4)$$

which sets the characteristic pressure on the sphere by the material. Assuming that Darcy-Reynolds pressure dominate all other forces, and that the intruder predominantly feels a frictional, decelerating force, the equation of motion can be written as

$$m\ddot{z} = -A\pi L^2 P_f, \quad (5)$$

where m is the intruder mass, z is the penetration depth, dots denote time derivatives, and A is an effective friction coefficient. We note that since all the dynamics involve deceleration of the intruder after impact, we denote $a = -\ddot{z}$ in our plots below and our scaling analysis of the maximum deceleration, a_{\max} .

B. Testable predictions from Darcy-Reynolds theory

The next step is to connect the shear length scale L with the penetration depth z of the intruder in order to close the equation of motion and predict dynamics, including scaling laws. This requires using the specific geometry of the intruder shape. For a spherical intruder, the contact area is circular and L is set by the radius of this circular contact boundary between the spherical intruder and the bed, which grows nonlinearly with z . If the Darcy-Reynolds pressure is very large, then the penetration depth of the sphere is small, i.e., $z \ll D$ (this is observed experimentally for small grains). In this case, simple geometry with a small-angle approximation yields $L^2 \approx Dz$. This approximation is specific to spherical intruders, meaning that other shapes would require a different calculation connecting L and z . Inserting this approximation into Eq. (5) yields

$$\frac{\pi}{6} \rho_s D^3 \ddot{z} = -\frac{\pi A \alpha \eta_f D^{3/2} \Delta \phi}{d^2} z^{3/2} \dot{z}, \quad (6)$$

where $\Delta \phi = \phi - \phi_c$. The effective mass density ρ_s can be defined as $\rho_s \equiv 6m/\pi D^3$, where D is the sphere diameter. After integrating in time, Eq. (6) yields a dimensionless equation of motion

$$d\tilde{z}/d\tilde{t} = -(2/5)\tilde{z}^{5/2} + 1, \quad (7)$$

where $\tilde{z} = z/Vt_m$, $\tilde{t} = t/t_m$, and

$$t_m = \frac{D}{V} \left(6A\alpha \frac{\eta_f D}{\rho_s d^2 V} \Delta \phi \right)^{-2/5}. \quad (8)$$

The initial conditions are given by $z(0) = 0$ and $\dot{z}(0) = V$, where V is the initial velocity at impact. This means that the dimensionless velocity at impact is $\tilde{V} = 1$, since $d\tilde{z}/d\tilde{t} = \dot{z}/V$ and $\dot{z} = V$ at initial impact.

Numerically solving Eq. (6) yields a deceleration vs time curve that rises, peaks at characteristic time set by t_m , and decreases. Such a curve can be seen in the Supplemental Material of Ref. [21] as well as in comparison to our experimental data in Fig. 2(b) (dashed line). The peak dimensionless acceleration $\tilde{a}_{\max} = a_{\max} t_m / V$ is therefore

$$a_{\max} \propto \frac{V}{t_m} = \frac{V^2}{D} \left(6A\alpha \frac{\eta_f D}{\rho_s d^2 V} \Delta \phi \right)^{2/5}. \quad (9)$$

This equation predicts, for example, a peak force scaling via $a_{\max} \propto d^{-0.8} \eta_f^{0.4} V^{1.6}$, which can be explicitly tested.

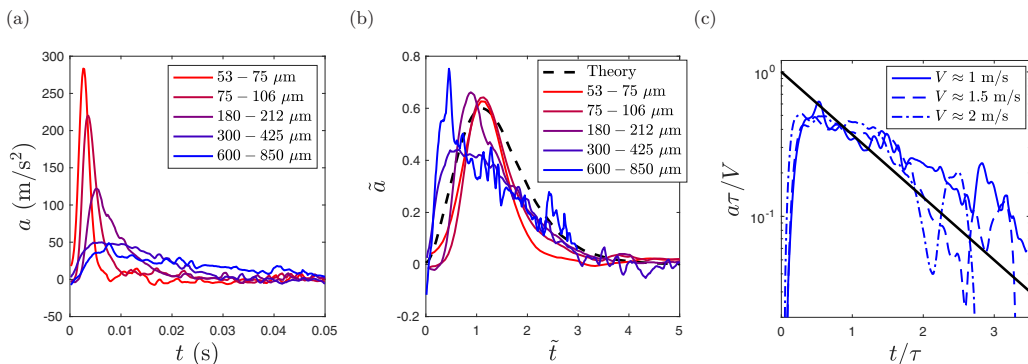


FIG. 2. Experimental data for impacts into mixtures of water, $\eta_f = 1$ cp, and glass beads of varying diameter d , using an intruder of diameter $D = 20$ mm and mass $m = 0.047$ kg. (a) Acceleration $a = -\ddot{z}$ as a function of time for impacts with similar impact speed, $V \approx 1$ m/s, for each of the five values of d . (b) Dimensionless acceleration \tilde{a} as a function of dimensionless time \tilde{t} , as defined in Eq. (7). Smaller grains collapse well, where the assumptions leading up to this equation are valid. (c) Three representative curves of acceleration vs time for the largest beads (600 to 850 μm), where the assumptions for Eq. (7) are not valid. These larger grains are better captured by Eq. (11).

The derivation of Eq. (9) contains several assumptions. The breakdown of the validity of these assumptions leads to measurably different scaling behaviors. One assumption discussed by Jerome *et al.* is that ϕ_c can be strain rate dependent, shifting the solidification response *during* impact. Other deviations are possible; for example, in the case that the Darcy-Reynolds pressure is not sufficiently large to preserve $z \ll D$ throughout the impact, then Eq. (6) onward must be reevaluated. In the case where the Darcy-Reynolds pressure is dominant but still small enough that the penetration depth becomes similar to or larger than D , the contact area is simply proportional to the intruder cross-sectional area, meaning that $L \approx D$, not $L \approx \sqrt{Dz}$. This means that Eq. (6) becomes

$$\ddot{z} = -\frac{6A\alpha\eta_f\Delta\phi}{\rho_s d^2}\dot{z}. \quad (10)$$

Thus, in this limit, the force on the impacting sphere is proportional to its speed, suggesting $a_{\text{max}} \propto V$. Note that this linear dependence on velocity is reminiscent of Stokes drag, although the physical mechanism is different.

Equation (10) predicts exponential decay in the velocity and acceleration, specifically

$$\ddot{z} = -\frac{V}{\tau}e^{-t/\tau}, \quad (11)$$

where $\tau = \frac{\rho_s d^2}{6A\alpha\eta_f\Delta\phi}$. However, we note that during the initial stages of penetration, $L^2 \approx Dz$ would still be valid, so we expect a buildup of the force before exponential decay takes over as the intruder passes through different scaling regimes. The equations in this section contain specific predictions about the dynamics, which are testable via experiments, as we show below. We note that there are other assumptions in these equations which may not always be valid, such as the assumption that A is a constant that is independent of any system parameter. This and other assumptions may be responsible for deviations from these predictions, as we discuss below.

III. EXPERIMENTAL METHODS

To test the predictions from the previous section, we perform experiments where a spherical intruder of mass $m = 0.047$ kg and diameter $D = 0.02$ m is dropped into fluid-saturated granular beds. The dependence on $\Delta\phi$ was carefully confirmed in Ref. [21]. Instead, we focus on other

parameters, specifically V , d , and η_f . We note that Jerome *et al.* [21] included selected results where these parameters were varied in order to demonstrate trends that were consistent with the DRT picture. We use five distinct sets of glass beads (Mo-Sci), with d ranges of (1) 53–75 (mean of 64), (2) 75–106 (mean of 90.5), (3) 180–212 (mean of 196), (4) 300–425 (mean of 362.5), and (5) 600–850 (mean of 725) in units of μm . Details of the fluids are described below.

We note that we did not have the experimental means to carefully prepare an homogeneous packing for each drop at a precise value of ϕ . Thus, our rationale was to use a simple, repeatable experimental protocol that assumed that the bed had a positive value of $\Delta\phi$ and that this value did not change significantly across different experiments, or at least that fluctuations in $\Delta\phi$ would be averaged out. We believe our experimental data justify this position as reasonable, as we discuss below.

A. Details of the fluids

We vary η_f in two ways. First, we add glycerol to water in various concentrations, using data from [35] to estimate the viscosity of the resulting mixture. By volume glycerol was diluted with water in 25% increments and then converted to mPas for data analysis. Using these increments we achieve viscosity of 1 mPas (water), 2.4 mPas (25% glycerol), 7.9 mPas (50% glycerol), 24 mPas (75% glycerol), and 1412 mPas (100%). All viscosity experimental data were collected in an ambient temperature between 21.7–24.4 °C, minimizing the impact of viscosity variance due to temperature variance. We note that glycerol is hygroscopic and that there can be a few percent ambiguity in the glycerol fraction in the mixtures. However, a small change in the glycerol fraction will not affect the viscosity of the fluid significantly, except perhaps for the 100% glycerol sample. If that were to have absorbed a few percent of water, its viscosity might drop by at most a factor three. In figures below, we include a horizontal error bar to highlight this uncertainty.

Due to data saving and resetting of the experiment, there were always several minutes that elapsed between any two individual impacts. We performed multiple tests to ensure that our experimental results for the high viscosity liquids were not sensitive to this settling process. We varied the time between experiments and performed subsequent series of drops where we went up in velocity for the first series and then back down for the second series. We additionally performed three representative impact experiments into the 100% glycerol mixture with settling times of 1, 2, and 24 h. The impacts with 24 h of settling did result in a roughly 20% increase in the peak acceleration measured during impact, but the impacts with 1 and 2 h settling had no discernible difference. We speculate that this is due to slow compaction of the bed over this time, caused by vibrations in the building or simple contact aging effects [36,37], which would increase ϕ and therefore increase the forces felt by the intruder. These data can be found in Ref. [38]. We note that we do not observe any bubbles (which were observed to play a role in Ref. [39]), but they would be hard to distinguish from the small particles we use.

Second, we use Ferrotec EFH1 Ferrofluid to conduct similar test to the glycerol, where we increase the viscosity by applying an external magnetic field. The ferrofluid has a base viscosity of 6 mPas [40], and we increase the viscosity by adding an external magnetic field using arrays of permanent magnets as well as a large solenoid for smaller adjustments. We use neodymium magnets that were arranged symmetrically on two (lateral) sides of the container holding the mixture of ferrofluid and glass beads. There was a gap (roughly 7.5 cm) between the magnet arrays and the sides of the container. The result was a magnetic field that was pointing in a direction orthogonal to the vertical direction (i.e., the direction of motion of the intruder). We used a Hall probe to measure the value of the magnetic field, before inserting the container filled with ferrofluid-grain mixture, at the point where the intruder would strike the surface of the material. This value is reported as B_0 when we present the results. We also move the Hall probe laterally along the direction of the magnetic field over the width of the container and observe an increase in the magnetic field of less than 50% of the value at the impact point. We estimate the variation in the field value in the region of intruder impact as less than 10%. We take data for $B_0 = 0$ mT (no field), 3, 9, 14, and 31 mT. Based

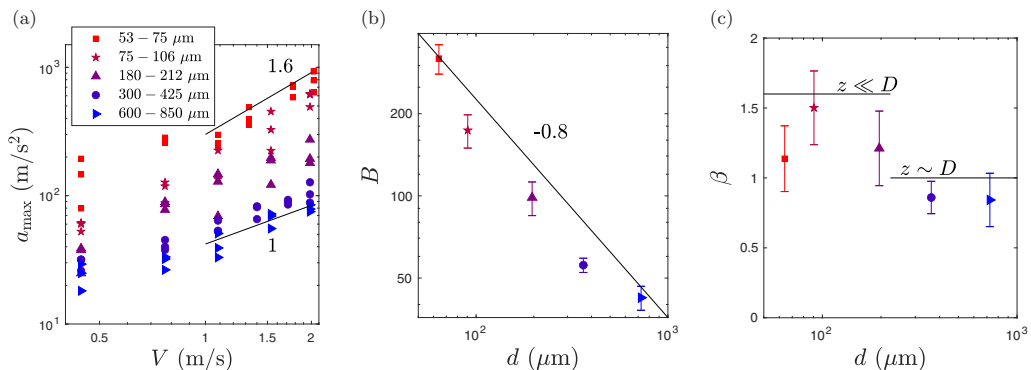


FIG. 3. Experimental data for impacts into mixtures of water, $\eta_f = 1$ cp, and glass beads of varying diameter d , using an intruder of diameter $D = 20$ mm and mass $m = 0.047$ kg. (a) a_{\max} vs V for all five values of d . Smaller beads obey the scaling law in Eq. (9), as expected, since $z \ll D$ for these impacts. Larger beads obey $a_{\max} \propto V$ from Eq. (11), as expected, since $z \sim D$ for these impacts. (b, c) We perform linear fits to the logarithmic data in panel (a) to obtain the best fit for the function $a_{\max} = BV^\beta$. DRT predictions are shown: $B \propto d^{-0.8}$ for panel (b); $\beta = 1.6$ for small beads and $\beta = 1$ for large beads in panel (c).

on Ref. [41], we estimate that viscosity will increase by roughly two orders of magnitude over this range of B_0 . We return to this point below in Sec. IV, when we describe results from impacts into ferrofluid-saturated beds.

We note that the ferromagnetic particles that are suspended in the ferrofluid are orders of magnitude smaller than the glass beads. Additionally, impacts into the mixture of ferrofluid and glass beads are nondamaging to the beads themselves. To illustrate this, we show SEM images in Fig. 1(d) of the ferrofluid-grain mixture after letting a sample of the mixture sit out to dry. The silica beads are covered in ferrofluid particles, which appear as a continuous material on the length scale of a glass bead. Additionally, the glass beads are not damaged after being subjected to impacts.

B. Sample preparation

Samples are prepared by filling a 8×8 cm acrylic container with an open top with the relevant fluid to a level of roughly 10 cm. We then pour particles of given size until the particle packing level is at approximately the same height as the fluid. After this, we perturbed the bed by smoothing and stirring the particles using a small spoon, then removed and weighed any excess fluid from the top. By weighing both the fluid and the grains as they are poured, we can estimate the volume ratio and thus packing fraction of the suspension. We observe $\phi \approx 0.59$ for all samples with the exception the largest beads ($d = 600$ to 850 μm), where $\phi \approx 0.60$ is found. We assume that $\phi > \phi_c$, which is corroborated by the fact that we observe a strong solidification during impact, consistent with the results for $\phi > \phi_c$ in Ref. [21]. If we also assume that $\phi_c \approx 0.585$, as measured by Jerome *et al.*, then this puts our beds somewhat above ϕ_c .

After each impact, we push displaced grains back to the crater and smooth the top surface using a small spoon. We find that the global packing fraction does not change during the course of many impacts. We take multiple data sets per bed going up in drop height (and therefore impact velocity) and then back down again, represented by the multiple data points in Fig. 3(a) for each impact velocity V . Additionally, we note that the intruder does not penetrate deep into the bed for all impacts except large grains with water (certainly not for the higher viscosity experiments), so removing the intruder does not significantly disturb most of the bed. Thus, if our bed were too loose at first, this would quickly be destroyed in the first few impacts. We find that our results are very repeatable, meaning that this issue is not a concern. Thus, we conclude that our measurements are in the $\Delta\phi > 0$

regime with values of $\Delta\phi > 0$ that do not change significantly, or are at least averaged out over small variations through multiple impacts at each value of V .

This protocol also depends somewhat on the fluid used. For water-based suspensions, any excitation from stirring quickly dissipates. For the more viscous samples, any stirring is challenging to do without introducing bubbles or transient bed states. To ensure that bed settling was not a dominant factor, additional experiments were performed to ensure that ϕ does not change significantly from run to run via the application of the protocol. Visual inspection shows that ϕ did not change in any significant manner until after many hours to days of settling. Impact experiments for high-viscosity glycerol-water mixtures were repeated over several hours and up to five days. The results showed that the impact-induced forces were quantitatively indistinguishable within the first 2 h. For very long settling times, the measured forces during impact increased by roughly 30% after one day of settling and roughly doubled after five days of settling [38]. However, all experiments conducted on the same day were found to give similar results. All the impact data shown here were collected in less than 4 h. We further verify that ϕ is not playing a role in our measurements by the fact that there is no significant change in the small fluid layer at the top of the sample. We also perform multiple sets of experiments with the same sample, and we find that our measurements are repeatable.

C. Generating impacts

A steel sphere is fixed to the end of a threaded rod and dropped from various heights H by releasing them using an electromagnet. Impact velocities are inferred by $V = \sqrt{2gH}$, where g is the gravitational acceleration; we also confirm these velocities using high-speed video for selected cases. We measure the acceleration using an onboard accelerometer (Sparkfun with ADXL377 with 500 Hz bandwidth). The accelerometer is wired to a data acquisition board with 32 AWG thin copper cables, which limits the range of H we can explore but was thin enough not to interfere with free fall motion of the intruder. A sketch of the setup is shown in Fig. 1(a).

We include in Supplemental Material [42] five representative videos of these impacts, taken with a Phantom V711. These videos include a representative video of (1) our smallest particles in water, showing a strong Darcy-Reynolds response; (2) our largest particles in water, showing essentially no Darcy-Reynolds response; (3, 4, and 5) our second-smallest particles in 25%, 75%, and 100% glycerol solutions, respectively. We refer to these videos throughout the remainder of the paper.

IV. RESULTS

A. Phenomenology

Figure 2(a) shows $a(t)$ for five impacts, one for each range of d , all with impact velocity $V \approx 1.1 \pm 0.1$ m/s. These curves clearly demonstrate that, consistent with the Darcy-Reynolds picture, smaller d leads to more sharply peaked deceleration profiles with larger values of a_{\max} . This is also supported by Supplemental Videos 1 and 2 [42], which show impacts into glass beads and water mixtures with mean particle diameters of $d = 64$ and $725 \mu\text{m}$, respectively. For the small particles, the intruder stops abruptly on impact. In contrast, it penetrates deeply into the bed of larger particles. Figure 2(b) shows $-\tilde{a}$, where $\tilde{a} \equiv d^2\ddot{z}/d\tilde{t}^2$, plotted as a function of \tilde{t} for each of the five curves shown in Fig. 2(a). For the three smallest particle size ranges ($d = 53\text{--}75 \mu\text{m}$, $d = 75\text{--}106 \mu\text{m}$, and $d = 180\text{--}212 \mu\text{m}$), the Darcy-Reynolds pressure is sufficiently large that $z \ll D$ is satisfied during the bulk of the trajectory, meaning that Eq. (9) is valid. The rescaled experimental results for the smaller values of d agree well with a numerical solution of Eq. (7), which is shown as a black dashed line.

To rescale the experimental data in Fig. 2(b), we need to set t_m for each curve. Several parameters in t_m are not directly measurable or known *a priori*, but a suitable collapse (at least for small d) is found by setting $6A\alpha\Delta\phi = 80$. The packing fraction differential $\Delta\phi$ is of order 10^{-2} , meaning that the product $A\alpha$ is of order 10^3 . Above, we estimated $\alpha \approx 20$, meaning that the effective friction coefficient $A \approx 50$. While this value appears very high for a friction coefficient, we note that it is

not a simple friction coefficient and that a previous study on granular intrusion found a value of approximately 35 for a similar parameter [43]. Additionally, we note that the assumptions leading up to Eq. (4) may affect the value of α . In any case, the quantities are within reasonable physical bounds, and assuming $6A\alpha\Delta\phi = 80$ yields good agreement between the experimental trajectories and the theoretical prediction of Eq. (9) for small d .

In contrast, for the two largest particle sizes, the Darcy-Reynolds pressure is much smaller, meaning that the sphere is able to penetrate more deeply into the material (see Supplemental Video 2 [42]). In this case, $z \ll D$ is not satisfied, so it is not surprising from the theoretical prediction that arises from solving Eq. (7) numerically that the experimental results do not match the Jerome predictions. This argument can be made quantitative by estimating the penetration depth z^* at peak deceleration in the following way. By assuming that the average deceleration between $t = 0$ and the time t_{\max} corresponding to the peak deceleration is equal to half of the peak value (corresponding to approximating the rise in deceleration as linear), then $z^* \approx Vt_{\max} - a_{\max}t_{\max}^2/4$. We can then use z^*/D as a dimensionless measure of how far the sphere has penetrated relative to its own diameter at t_{\max} . For the smallest particles, with $d = 53\text{--}75 \mu\text{m}$, we find typical values of $z^*/D \sim 0.1$, meaning that $z \ll D$ is a reasonable approximation. For the largest particles, with $d = 600\text{--}850 \mu\text{m}$, we find typical values of $z^*/D \sim 1$ or larger.

The data for $d = 600\text{--}850 \mu\text{m}$ in particular appear to be better described by a sharp rise followed by quasiexponential decay, consistent with Eq. (11). Figure 2(c) shows acceleration vs time for three impacts into beds with $d = 600\text{--}850 \mu\text{m}$ and with initial velocities $V \approx 1, 1.5,$ and 2 m/s ; the data for $V \approx 1$ are the same curve shown in Fig. 2(a). Note that the axes are rescaled using $\tau = \frac{\rho_s d^2}{6A\alpha\eta_f\Delta\phi}$, as defined in conjunction with Eq. (11), as well as the impact velocity V on the horizontal axis. The solid black line shows the theoretical prediction from Eq. (11). Note that the values used in the rescaling here are fully determined by the collapse in Fig. 2(b), using $6A\alpha\Delta\phi = 80$, leaving no free parameters.

B. Scaling results for V and d

Figure 3(a) shows a_{\max} vs V for all five particle sizes. Equation (9) shows that DRT predicts $a_{\max} \propto V^{1.6}$, under several assumptions, including $z \ll D$. Experimental results are more consistent with this prediction for smaller d (red squares, green stars, and black triangles) and larger V where these assumptions are valid. For large d (e.g., blue circles and magenta triangles), we observe $a_{\max} \propto V$, as predicted by Eq. (11) and consistent with the collapse in Fig. 2(c). Figures 3(b) and 3(c) show the result of fits to the a_{\max} vs V data in Fig. 3(a) of the form $a_{\max} = BV^\beta$ (error bars represent 95% confidence intervals). We find good agreement with the prediction from Eq. 9 that $B \propto d^{-0.8}$. The best fit for the exponent β is consistently smaller than the prediction of $\beta \approx 1.6$ from Eq. (9), even for small d where we would expect it to be valid. However, we note that the low value of β for the smallest particles seems to be caused by outliers at low V ; the large- V data appear very consistent with $\beta \approx 1.6$. Overall, $a_{\max} \propto V^{1.6}$ appears to be highly consistent with the data at small d . For larger d , where the Darcy-Reynolds pressure is smaller and we expect Eq. (11) to be applicable, we find $a_{\max} \propto V$ as expected. Overall, our data for varied d agree well with the predictions of DRT.

C. Viscosity dependence

Turning now to the impact behavior for varied η_f , Fig. 4 shows results for impacts at varying V and η_f with constant particle size $d = 75\text{--}106 \mu\text{m}$. Figure 4(a) shows typical acceleration curves with similar $V \approx 1.2$ but with varied η_f . The solid curves represent water-glycerol mixtures, and the dash-dotted curve (6 cp) represents the ferrofluid with no applied magnetic field. These curves appear qualitatively similar to those in Fig. 2. However, in contrast with the predictions of DRT, the peak value a_{\max} shows nonmonotonic behavior as η_f is increased: a_{\max} increases with η_f up to $\eta_f = 7.9 \text{ cp}$ but then decreases dramatically as η_f is further increased. This decrease in a_{\max} is qualitatively inconsistent with DRT. This behavior is corroborated by Supplemental Videos 3,

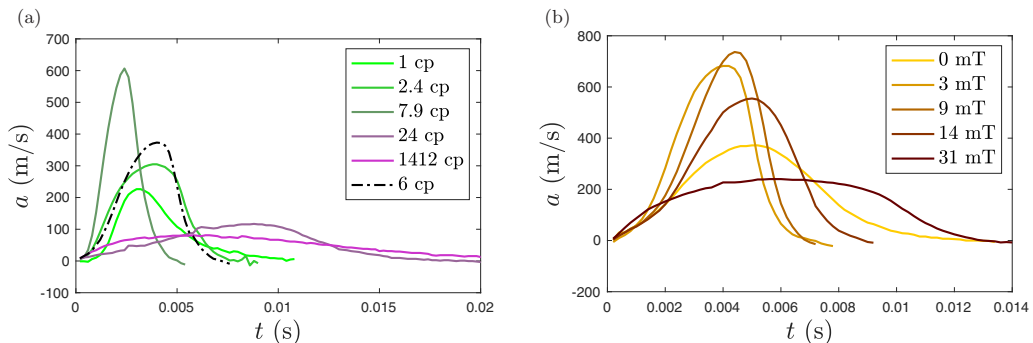


FIG. 4. Acceleration vs time for different impacts into beds with $d = 90 \mu\text{m}$ and varying fluid viscosity using an intruder of diameter $D = 20 \text{ mm}$ and mass $m = 0.047 \text{ kg}$. (a) Impacts with $V \approx 1$ where η_f is varied by adding glycerol to water. (b) Impacts with $V \approx 2.5$ where η_f is varied by using a ferrofluid and changing the external magnetic field. A zero-field ferrofluid impact result is also shown in panel (a) for the ferrofluid (dash-dotted line).

4, and 5 [42], which show impacts into 25%, 75%, and 100% glycerol solutions, respectively. The dynamics for impacts into the 25% and 75% solutions look similar, despite wildly different viscosities. The video of impact into the 100% glycerol solution shows the least abrupt deceleration, consistent with Fig. 4. Note that the stopping dynamics for the impact into the 100% glycerol solution are still much more abrupt than the impact into the $d = 725 \mu\text{m}$ beads and water, shown in Supplemental Movie 2 [42].

As stated in Sec. I, one motivation of these experiments was to move toward tunable particle-fluid mixtures. In particular, if the viscous fluid were replaced with a ferrofluid, then the particle-fluid mixture could be strengthened *in situ* by applying an external magnetic field. Our results for glycerol-water mixtures, shown in Fig. 4(a), suggest that this may not always be the case. Figure 4(b) shows that the breakdown of thickening at higher viscosities also occurs when the viscous fluid is no longer glycerol-water mixtures but is instead replaced by a ferrofluid. The initial viscosity of the ferrofluid is $\eta_f = 6 \text{ cp}$, which is just below the value of $\eta_f \approx 10 \text{ cp}$ where we expect to see

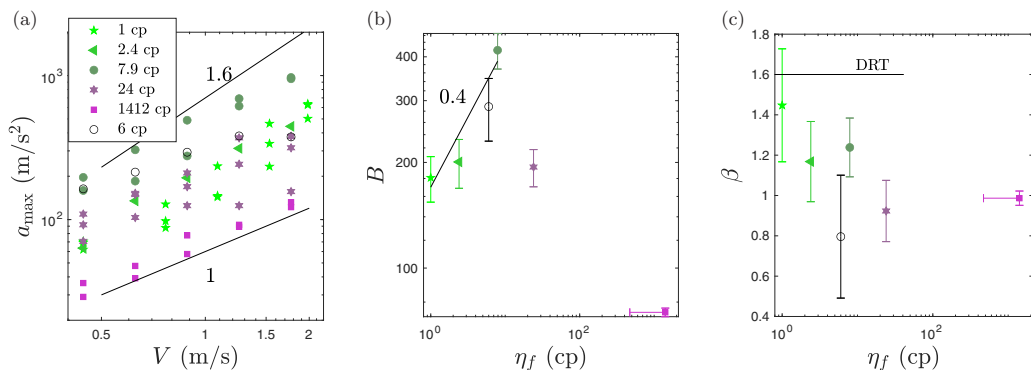


FIG. 5. Experimental data for impacts into mixtures with varied η_f and $d = 90 \mu\text{m}$ using an intruder of diameter $D = 20 \text{ mm}$ and mass $m = 0.047 \text{ kg}$. (a) a_{max} vs V for all values of η_f . (b), (c) We perform linear fits to the logarithmic data in panel (a) to obtain the best fit for the function $a_{\text{max}} = BV^\beta$. DRT predictions are shown: $B \propto \eta_f^{0.4}$ for panel (b); $\beta = 1.6$ in panel (c). Similar to the data from Fig. 4, we find that DRT breaks down for $\eta_f > 10 \text{ cp}$, and forces begin to decrease with increasing viscosity. The horizontal error bar represents the uncertainty in the viscosity for the 100% glycerol, as discussed in Sec. III A.

the largest values of a_{\max} for the range of V we study here. Therefore, we expect that as the applied magnetic field is increased, we should see a slight increase in a_{\max} followed by a decline. Figure 4(b) shows five curves of $a(t)$ with similar $V \approx 2.5$ m/s with five different magnetic field strengths, $B_0 = 0, 3, 9, 14,$ and 31 mT. We again find that a_{\max} increases with η_f (which we vary indirectly through B_0) and then begins to decrease. Importantly, we find this result consistently for all values of V . Figure 5(a) shows data for a_{\max} vs V . The data for $\eta_f = 1$ cp (water), marked with green stars, are the same data shown with deep red stars in Fig. 3. Figures 5(b) and 5(c) show results of best fits to these data in the form $a_{\max} = BV^\beta$. We again find that best fits for β tend to be slightly smaller than the prediction of $\beta = 1.6$ from Eq. (9). The best fits for B increase in a way that is consistent with the prediction of $B \propto \eta_f^{0.4}$ from Eq. (9) for 1 cp (water), 2.4 cp (25% glycerol), 6 cp (zero-field ferrofluid), and 7.9 cp (50% glycerol). However, for larger values of η_f , we observe that B begins to decrease, consistent with Fig. 4.

V. ANALYSIS OF ANOMALOUS VISCOSITY DEPENDENCE

Our results from the previous section suggest that DRT, a theory that explicitly describes transient phenomena, must be somehow modified in the limit of large viscosity interstitial fluid. We propose as an hypothesis that the frictional behavior of the grain-grain contacts is rate-dependent in a way that depends on the viscosity of the fluid. For the initial static packing, we assume all particles are making solid-solid contact, so all contacts are fully frictional. During the impact-induced shear, particles begin moving past one another and forming new contacts, which are implicitly assumed to have the same friction coefficient as the contacts from the original static packing. DRT then predicts that the packing will undergo a transient expansion phase due to Reynolds dilatancy, which gives rise to large Darcy forces. However, if the particles move past each other sufficiently quickly such that they are unable to squeeze out the viscous fluid between them and make solid-solid (frictional) contact, they may instead behave as frictionless contacts mediated through a lubrication layer.

Even a partial disruption in the frictional behavior between particles could have measurable effects on the observed impact dynamics. Reynolds dilatancy of the granular phase is an inherently frictional effect that does not exist for frictionless particles at all [44]. Additionally, the value of ϕ_c is strongly dependent on grain-grain friction and would increase if the grain-grain friction decreased [45], making $\Delta\phi$ smaller. So, if the grain-grain friction coefficient were *dynamically* reduced in this way, then the Darcy-Reynolds effect would also be reduced. This mechanism is somewhat similar to the mechanism that is often invoked to explain discontinuous shear thickening of dense suspensions [9,46,47], where friction “turns on” for sufficient applied shear stress. Our impact-induced lubrication hypothesis is one view that plausibly explains the data we show in Figs. 4 and 5.

Further work is certainly needed to better explore this hypothesis, including better accounting of the forces on individual particles and corresponding dimensional analysis. To highlight this, we note that Supplemental Movie 3 from Jerome *et al.* [21] shows a strong Darcy-Reynolds response for impact of spherical intruder of diameter $D = 25$ mm with $V = 2.55$ m/s into 1.3 mm spheres and silicone oil with $\eta_f = 100$ cp (or 0.1 Pa s). Although it is hard to tell just by the video whether the response obeys the predicted scaling, this viscosity is larger than the viscosity where we see anomalous scaling appear. Comparison with our results would require using at least one dimensionless number. The simplest choice would be either the Stokes number $St = \rho_g U d / \eta_f$, where ρ_g is the mass density of a grain and U is a characteristic speed, or the particle Reynolds number, $Re_p = \rho u d / \eta_f$, where ρ is the mass density of the fluid. We note that $St = (\rho_g / \rho) Re_p$, so $St \sim Re_p$ here, since $\rho_g / \rho \approx 2.5$ for soda-lime glass beads and water. Both numbers have been used to capture the ratio of inertial to viscous effects in the context of a small particle approaching a wall [48,49] or of particle-particle collisions in a viscous fluid [50]. In particular, Yang and Hunt [50] showed that, for large St , restitution losses were similar to the dry case. For $St < 100$, the restitution coefficient decreased and approached zero at $St \sim 10$. In the present case, these dimensionless

numbers could be used to quantify the dynamics of inertial particles overcoming lubrication forces to make frictional contact.

To determine the values of St and Re_p where anomalous scaling begins, one approach would be to set U as simply the impact speed V . In this case, the anomalous scaling we observe appears for $\eta_f > 10$ cp with $d = 90 \mu\text{m}$ and typical impact velocities of $V = 1$ m/s. This corresponds to $Re_p < 11$. The video referenced above from Jerome *et al.* [21] would have $Re_p \approx 32$, which is above the value where we observe anomalous behavior, so a strong Darcy-Reynolds response is consistent. The value of $Re_p \sim 10$ has the advantage of being similar to the value where the restitution coefficient went to zero in the study by Yang and Hunt [50]. However, it is likely that velocity scale U is not the absolute velocity scale V set by the intruder, but the typical relative velocity between two particles. Assuming that the velocity goes to zero over the size of the shear zone L , then $U \approx V(d/L)$. If we assume $L \approx D$, then this reduces Re_p by a factor $d/D \approx 1/200$ in our experiments and $1/20$ for the case shown by Jerome *et al.* [21], separating the two cases even more. In any case, future experiments and theoretical work is needed to fully understand how and why DRT should be modified in the limit of small particles and large viscosity.

VI. CONCLUSION

Here we have followed Jerome *et al.* [21] to derive equations describing the dynamics of a sphere impacting a fluid-saturated granular bed, where the granular phase is compacted above the critical volume fraction such that it dilates under shear. The dilation (Reynolds) caused by the impact forces fluid to flow into the expanding pore structure, and the resulting Darcy pressure dominates the force on the intruder. We have expanded on the derivation from Ref. [21] to include the case where the sphere penetration depth becomes similar to or larger than its diameter.

The predictions from this theory were experimentally confirmed by Jerome *et al.* [21] with regard to the dependence on $\Delta\phi$. Here we performed additional experiments to test the theory's predictions on other parameters, specifically impact velocity V , particle size d , and fluid viscosity η_f . Our experimental results confirm the predictions of DRT for variation in d over more than an order of magnitude. For small d , DRT as formulated in Ref. [21] works well. For larger d , a key approximation ($z \ll D$) for the context of impact dynamics is no longer applicable, so the equation of motion describing the impacting sphere's dynamics must be modified. However, with this modification, DRT still captures the observed behavior over a large range of d .

When we vary η_f , we observe good agreement with DRT for η_f between 1 and 10 cp, specifically that $a_{\text{max}} \propto \eta_f^{0.4}$. However, for $\eta_f > 10$ cp (and other details of the experiment held constant, such as particle diameter $d = 90 \mu\text{m}$), we observe that forces generated during impact begin to decrease as η_f is further increased. We validate this result with two methods: varying η by adding glycerol to water as well as by using a ferrofluid with an externally applied magnetic field. Both approaches show that the forces generated during impact begin to decrease with increasing η_f at $\eta_f \approx 10$ cp. This is qualitatively inconsistent with DRT, suggesting that a new theory, or at least some modification, is required. We hypothesize that this effect is controlled by the particle Reynolds number Re_p and the anomalous behavior occurs when $Re_p < 10$. Future work is required to better explore this phenomenon.

Finally, as pointed out in [21], the pore-pressure effects from DRT could help explain the dramatic response of impact into shear-thickening suspensions. Shear-thickening suspensions differ from saturated granular beds, in that the particles are not making solid-solid contact in the absence of driving. However, in these systems, ϕ_c decreases as stress is applied, causing dilation and thereby inducing a large Darcy pressure that solidifies the material. We emphasize that there are key differences between the system discussed here and impact into dense suspensions. For example, in the initial state of the system before impact, the particles in DRT experiments are making solid-solid contact in a dense packing. In impacts into dense suspensions, the particles begin in a state whereby they are not making contact with each other but are "suspended" in the liquid. Additionally, in the theoretical analysis discussed here, there is no propagation time between the intruder and the shear

flow in the material below it. This is apparent from the fact that the shear length L is set by the current value of the contact radius between the intruder and bed, as opposed to the value of the contact radius at some previous time. For impacts into dense suspensions, propagation phenomena are thought to play a key role in the impact response of shear-thickening suspensions [12,14,34,51] but are not considered in DRT. However, DRT likely plays an important role in impact behavior into shear-thickening suspensions, primarily by holding together the dynamic solidlike region often observed in experiments on impact into shear-thickening suspensions.

ACKNOWLEDGMENTS

We acknowledge funding from the Office of Naval Research under Grant No. N0001419WX01519 and by the Office of Naval Research Global Visiting Scientist Program VSP 19-7-001. We thank Drago Grbovic for taking SEM images.

-
- [1] K. N. Nordstrom, D. S. Dorsch, W. Losert, and A. G. Winter, V, Microstructural view of burrowing with a bioinspired digging robot, *Phys. Rev. E* **92**, 042204 (2015).
 - [2] A. Kudrolli and B. Ramirez, Burrowing dynamics of aquatic worms in soft sediments, *Proc. Natl. Acad. Sci. USA* **116**, 25569 (2019).
 - [3] S. Gürgen, M. C. Kuşhan, and W. Li, Shear thickening fluids in protective applications: A review, *Prog. Polym. Sci.* **75**, 48 (2017).
 - [4] F. Boyer, E. Guazzelli, and O. Pouliquen, Unifying Suspension and Granular Rheology, *Phys. Rev. Lett.* **107**, 188301 (2011).
 - [5] M. Trulsson, B. Andreotti, and P. Claudin, Transition from the Viscous to Inertial Regime in Dense Suspensions, *Phys. Rev. Lett.* **109**, 118305 (2012).
 - [6] E. Guazzelli and O. Pouliquen, Rheology of dense granular suspensions, *J. Fluid Mech.* **852**, P1 (2018).
 - [7] T. Pähz, O. Durán, D. N. de Klerk, I. Govender, and M. Trulsson, Local Rheology Relation with Variable Yield Stress Ratio across Dry, Wet, Dense, and Dilute Granular Flows, *Phys. Rev. Lett.* **123**, 048001 (2019).
 - [8] E. Brown and H. M. Jaeger, Shear thickening in concentrated suspensions: Phenomenology, mechanisms and relations to jamming, *Rep. Prog. Phys.* **77**, 046602 (2014).
 - [9] M. Wyart and M. E. Cates, Discontinuous Shear Thickening without Inertia in Dense Non-Brownian Suspensions, *Phys. Rev. Lett.* **112**, 098302 (2014).
 - [10] R. Seto, R. Mari, J. F. Morris, and M. M. Denn, Discontinuous Shear Thickening of Frictional Hard-Sphere Suspensions, *Phys. Rev. Lett.* **111**, 218301 (2013).
 - [11] P. Umbanhowar and D. I. Goldman, Granular impact and the critical packing state, *Phys. Rev. E* **82**, 010301(R) (2010).
 - [12] S. R. Waitukaitis and H. M. Jaeger, Impact-activated solidification of dense suspensions via dynamic jamming fronts, *Nature (London)* **487**, 205 (2012).
 - [13] A. H. Clark, A. J. Petersen, L. Kondic, and R. P. Behringer, Nonlinear Force Propagation During Granular Impact, *Phys. Rev. Lett.* **114**, 144502 (2015).
 - [14] E. Han, I. R. Peters, and H. M. Jaeger, High-speed ultrasound imaging in dense suspensions reveals impact-activated solidification due to dynamic shear jamming, *Nat. Commun.* **7**, 12243 (2016).
 - [15] D. I. Goldman and P. Umbanhowar, Scaling and dynamics of sphere and disk impact into granular media, *Phys. Rev. E* **77**, 021308 (2008).
 - [16] I. R. Peters and H. M. Jaeger, Quasi-2d dynamic jamming in cornstarch suspensions: Visualization and force measurements, *Soft Matter* **10**, 6564 (2014).
 - [17] D. van der Meer, Impact on granular beds, *Annu. Rev. Fluid Mech.* **49**, 463 (2017).
 - [18] A. M. Walsh, K. E. Holloway, P. Habdas, and J. R. de Bruyn, Morphology and Scaling of Impact Craters in Granular Media, *Phys. Rev. Lett.* **91**, 104301 (2003).

- [19] J. S. Uehara, M. A. Ambroso, R. P. Ojha, and D. J. Durian, Low-Speed Impact Craters in Loose Granular Media, *Phys. Rev. Lett.* **90**, 194301 (2003).
- [20] N. Krizou and A. H. Clark, Power-Law Scaling of Early-Stage Forces during Granular Impact, *Phys. Rev. Lett.* **124**, 178002 (2020).
- [21] J. J. S. Jerome, N. Vandenberghe, and Y. Forterre, Unifying Impacts in Granular Matter from Quicksand to Cornstarch, *Phys. Rev. Lett.* **117**, 098003 (2016).
- [22] E. R. Nowak, J. B. Knight, M. L. Povinelli, H. M. Jaeger, and S. R. Nagel, Reversibility and irreversibility in the packing of vibrated granular material, *Powder Technol.* **94**, 79 (1997).
- [23] L. A. Pugnaloni, M. Mizrahi, C. M. Carlevaro, and F. Vericat, Nonmonotonic reversible branch in four model granular beds subjected to vertical vibration, *Phys. Rev. E* **78**, 051305 (2008).
- [24] P. A. Gago and S. Boettcher, Universal features of annealing and aging in compaction of granular piles, *Proc. Natl. Acad. Sci. USA* **117**, 33072 (2020).
- [25] B. Allen and A. Kudrolli, Granular bed consolidation, creep, and armoring under subcritical fluid flow, *Phys. Rev. Fluids* **3**, 074305 (2018).
- [26] O. Reynolds, LVII. On the dilatancy of media composed of rigid particles in contact. With experimental illustrations, *London Edinburgh Dublin Philos. Mag. J. Sci.* **20**, 469 (1885).
- [27] H. Darcy, *Les fontaines publiques de dijon ed 1856* (Hachette Livre-Bnf, Paris, France, 2012).
- [28] C. Li, T. Zhang, and D. I. Goldman, A terradynamics of legged locomotion on granular media, *Science* **339**, 1408 (2013).
- [29] S. Agarwal, A. Karsai, D. I. Goldman, and K. Kamrin, Surprising simplicity in the modeling of dynamic granular intrusion. *Sci. Adv.* **7**, eabe0631 (2021).
- [30] K. Raj, B. Moskowicz, and R. Casciari, Advances in ferrofluid technology, *J. Magn. Magn. Mater.* **149**, 174 (1995).
- [31] K. Sakaie, D. Fenistein, T. J. Carroll, M. van Hecke, and P. Umbanhowar, MR imaging of Reynolds dilatancy in the bulk of smooth granular flows, *Europhys. Lett.* **84**, 38001 (2008).
- [32] A. J. Kabla and T. J. Senden, Dilatancy in Slow Granular Flows, *Phys. Rev. Lett.* **102**, 228301 (2009).
- [33] V. V. Vasisht and E. Del Gado, Computational study of transient shear banding in soft jammed solids, *Phys. Rev. E* **102**, 012603 (2020).
- [34] M.-A. Brassard, N. Causley, N. Krizou, J. A. Dijkstra, and A. H. Clark, Viscous-like forces control the impact response of dense suspensions, *J. Fluid Mech.* **923**, A38 (2021).
- [35] J. B. Segur and H. E. Oberstar, Viscosity of glycerol and its aqueous solutions, *Ind. Eng. Chem.* **43**, 2117 (1951).
- [36] J. A. Dijkstra, G. H. Wortel, L. T. H. van Dellen, O. Dauchot, and M. van Hecke, Jamming, Yielding, and Rheology of Weakly Vibrated Granular Media, *Phys. Rev. Lett.* **107**, 108303 (2011).
- [37] V. B. Nguyen, T. Darnige, A. Bruand, and E. Clement, Creep and Fluidity of a Real Granular Packing near Jamming, *Phys. Rev. Lett.* **107**, 138303 (2011).
- [38] J. M. Strader, The effect of ferrofluid on a dilatant fluid's intrusion resistance, Master's thesis, Naval Postgraduate School, Monterey, CA, 2020.
- [39] B. Allen, B. Sokol, S. Mukhopadhyay, R. Maharjan, and E. Brown, System-spanning dynamically jammed region in response to impact of cornstarch and water suspensions, *Phys. Rev. E* **97**, 052603 (2018).
- [40] See datasheet for EFH Series Ferrofluid from Ferrotec Corporation (2018), <https://ferrofluid.ferrotec.com/wp-content/uploads/sites/3/efhsds.pdf>.
- [41] R. Patel, R. Upadhyay, and R. Mehta, Viscosity measurements of a ferrofluid: Comparison with various hydrodynamic equations, *J. Colloid Interface Sci.* **263**, 661 (2003).
- [42] See Supplemental Material at <http://link.aps.org/supplemental/10.1103/PhysRevFluids.7.054304> for videos of selected impacts, as described in the text.
- [43] T. A. Brzinski, P. Mayor, and D. J. Durian, Depth-Dependent Resistance of Granular Media to Vertical Penetration, *Phys. Rev. Lett.* **111**, 168002 (2013).
- [44] P.-E. Peyneau and J.-N. Roux, Frictionless bead packs have macroscopic friction, but no dilatancy, *Phys. Rev. E* **78**, 011307 (2008).
- [45] L. E. Silbert, Jamming of frictional spheres and random loose packing, *Soft Matter* **6**, 2918 (2010).

- [46] J. F. Morris, Toward a fluid mechanics of suspensions, [Phys. Rev. Fluids](#) **5**, 110519 (2020).
- [47] J. F. Morris, Shear thickening of concentrated suspensions: Recent developments and relation to other phenomena, [Annu. Rev. Fluid Mech.](#) **52**, 121 (2020).
- [48] H. Brenner, The slow motion of a sphere through a viscous fluid towards a plane surface, [Chem. Eng. Sci.](#) **16**, 242 (1961).
- [49] G. Joseph, R. Zenit, M. Hunt, and A. Rosenwinkel, Particle–wall collisions in a viscous fluid, [J. Fluid Mech.](#) **433**, 329 (2001).
- [50] F.-L. Yang and M. Hunt, Dynamics of particle-particle collisions in a viscous liquid, [Phys. Fluids](#) **18**, 121506 (2006).
- [51] E. Han, M. Wyart, I. R. Peters, and H. M. Jaeger, Shear fronts in shear-thickening suspensions, [Phys. Rev. Fluids](#) **3**, 073301 (2018).